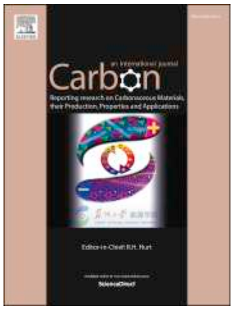

Nitrogen, oxygen and sulfur co-doped hierarchical porous carbons toward high-performance supercapacitors by direct pyrolysis of kraft lignin

Fangyan Liu, Zixing Wang, Haitao Zhang, Long Jin, Xiang Chu, Bingni Gu, Haichao Huang, Weiqing Yang

PII: S0008-6223(19)30350-1

DOI: https://doi.org/10.1016/j.carbon.2019.04.023

Reference: CARBON 14107

To appear in: *Carbon*

Received Date: 25 November 2018

Revised Date: 20 February 2019

Accepted Date: 6 April 2019

Please cite this article as: F. Liu, Z. Wang, H. Zhang, L. Jin, X. Chu, B. Gu, H. Huang, W. Yang, Nitrogen, oxygen and sulfur co-doped hierarchical porous carbons toward high-performance supercapacitors by direct pyrolysis of kraft lignin, *Carbon* (2019), doi: https://doi.org/10.1016/j.carbon.2019.04.023.

Graphical abstract

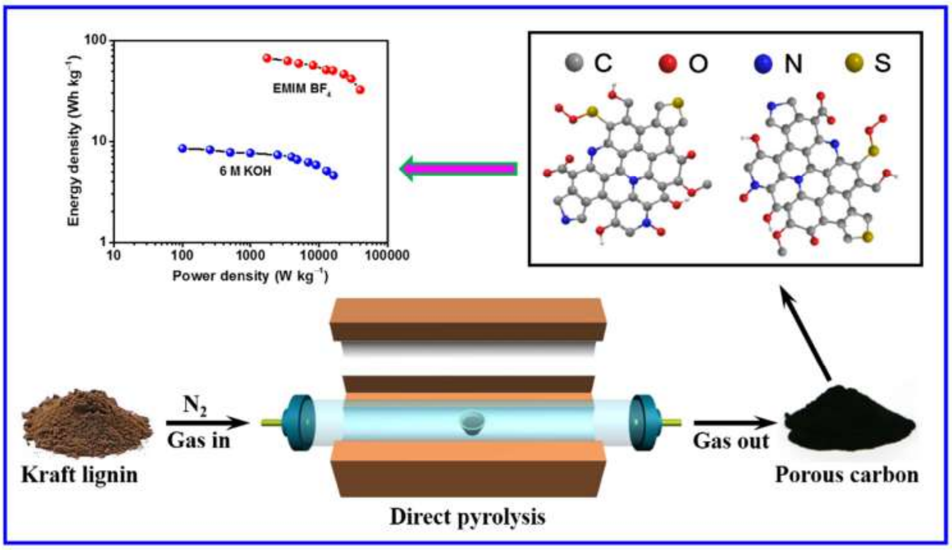

Nitrogen, oxygen and sulfur co-doped hierarchical porous carbons toward high-performance supercapacitors by direct pyrolysis of kraft lignin

Fangyan Liu, Zixing Wang, Haitao Zhang, Long Jin, Xiang Chu, Bingni Gu, Haichao Huang, Weiqing Yang*

Key Laboratory of Advanced Technologies of Materials (Ministry of Education); State Key Laboratory of Traction Power; School of Materials Science and Engineering, Southwest Jiaotong University, No. 111, North 1st Section of Second Ring Road, Jinniu District, Chengdu 610031, China.

---

[*] Corresponding author. Phone:028-87600415; E-mail: wqyang@swjtu.edu.cn

ABSTRACT:

The O-N-S co-doped hierarchical porous carbons is prepared by direct pyrolysis of kraft lignin which is the byproduct from papermaking black liquor. The proposed preparation method is extremely facile, green-environmental, and low-cost without any additional activating agent, additives or templates. The kraft lignin-derived carbon materials possess large specific surface areas (338−1307 m^2 g^{-1}), hierarchical porous structure and abundant multi-heteroatoms co-doping (9.84−19.91 wt%). Benefiting from above synergistic advantages, the as-fabricated symmetric supercapacitor in aqueous electrolyte delivers a high specific capacitance of 244.5 F g^{-1} at 0.2 A g^{-1}, excellent rate-capability (81.8% retention of initial capacitance at 40.0 A g^{-1}), and outstanding cycling stability (91.6% retention over 10000 cycles). Importantly, this device in aqueous electrolyte delivers an energy density of 8.5 W h kg^{-1} at a power density of 100 W kg^{-1}. Furthermore, a remarkable energy density of 66.8 W h kg^{-1} at a power density of 1.75 kW kg^{-1} has been achieved and 32.2 W h kg^{-1} is still maintained even at an ultrahigh power density of 40.0 kW kg^{-1} when ionic liquid serves as electrolyte. This study demonstrates the successful conversion of low-valued natural biomass derivative into sustainable high-performance supercapacitor electrode materials with a simple, low-cost, and green-environmental production process.

1. Introduction

Owing to steadily increasing environmental and energy crises causing by the sharp depletion of non-renewable fossil fuels, it is imperative to develop the high-performance energy storage systems such as supercapacitors and Li-ion batteries to satisfy the ever-growing demands for sustainable energy [1, 2]. As a primary and promising energy source, supercapacitors have gained enormous attention due to their outstanding attributes of higher power-delivery capability (10 kW kg^{-1}), faster charge–discharging rate (within second), and longer life stability ($>10^5$) than lithium-ion batteries [3-5]. As a type of primary and prospective electrode material, carbon materials including porous carbons (PCs) [6], activated carbons (ACs) [7], carbon nanotubes (CNTs) [8], carbon aerogels [9] and graphene [10] have shown the convincing merits of adjustable porosity, high specific surface area, non-toxicity, favorable physicochemical stability, and superior electronic conductivity [11, 12]. Encouragingly, carbon materials deriving from abundant, renewable and low-cost natural biomass instead of coal and fossil oil show more promising and practical value, especially from the sustainable, environmental and economic perspective.

However, the relatively low energy density of natural biomass-based carbon materials cannot make them keep up with the demands of practical applications [13]. To improve the electrochemical performance of supercapacitors based on the biomass-derived carbon materials, a typical and useful strategy is to produce the carbon-based electrode materials with the desirable features such as (i) hierarchical porous structure with the combination of abundant micro-, meso-, and macropores. Generally, the micropores and mesopores are beneficial for achieving high ion-accessible surface area, guaranteeing a large specific capacitance; the mesopores and macropores provide channels for ion rapidly-shuttling back and forth, resulting in a high rate capability, (ii) 3 D interconnected skeleton with excellent conductivity that renders the excellent electron pathways, and (iii) high-level heteroatom doping (N, O, P, or S) that improves wettability and conductivity as well as provides pseudocapacitance via Faradaic reactions. In this regard, most of hierarchical porous carbons (HPCs) were accessible by hard-/soft-template or non-template methods **[12]**. However, the template methods require expensive templates (ordered mesoscopic silica **[14]**, ice templating **[15]**, ice templating alongside the colloidal silica and physical activation **[16]**, etc.) and the complex follow-up treatment are usually time-wasting and environmentally hazardous. As for non-template method, physical/thermal (CO_2 **[17]** or water steam **[18, 19]**) and chemical activations (KOH **[20]**, NaOH **[21]**, H_3PO_4 **[22, 23]**, K_2CO_3 **[24]**, etc.) are necessary, leading to the high cost. To realize heteroatom doping into carbon skeleton, extra additives such as melamine [25], thiourea [26], polyphosphoric acid [27], and sulphur [28] are used, which further adds the production costs. Therefore, it is a big challenge to achieve the 3 D heteroatom-doped HPCs derived from natural biomass via a simple, cost-effective, and environmentally friendly method.

Lignin, the most abundant renewable aromatic compounds of plant biomass on earth [29], is primarily isolated as the byproduct of biorefinery and pulping and papermaking industry, and possesses attractive features such as inexpensive cost, high carbon content, biodegradability, good thermal stability [30, 31]. Kraft lignin, the main component recovered from the sulfate pulping black liquor which contains not only kraft lignin but also NaOH, Na_2S, Na_2SO_4, Na_2CO_3 and a small amount of other substances [30, 32]. However, the underutilization of the industrial lignin leads to a great deal of lignin directly burned off or even discharged into water resource as a waste, which causes serious environmental pollution and resource waste. Currently, increasing attention has been devoted for the preparation of high-performance carbon electrode materials from various lignin such as enzymatic hydrolysis lignin [33], kraft lignin [34, 35], ethanol-extracted lignin and diluted alkali lignin [35], steam explosion lignin [36, 37], and sodium lignosulfonate [38, 39]. However, to our best knowledge, the preparation processes of the lignin-derived carbons are usually complex such as hydrothermal carbonization-KOH activation, pyrolysis-KOH activation, etc, time-consuming with tedious processes, high-cost with additional additives (e.g. activation agents, template agents, and heteroatom-contained agents) or relatively simple but the obtained carbon materials feature with general electrochemical performance [1, 33-41]. Therefore, it is imperative to develop useful utilization approaches to convert the mass-produced industrial lignin into value-added and high-performance carbon materials by a rather simple, low-cost, and eco-environmental approach.

In this work, we prepare the O, N, S co-doped hierarchical porous carbons (ONS-HPCs) with high electrochemical performances via an extremely simple, green-environmental, and low-cost method that is the direct self-activated pyrolysis of the kraft lignin. No activation steps, template agents or other additional additives were employed and only one step was adopted in the preparation process. The morphology, structure, and chemical information of the produced carbon materials have been systematically investigated. Impressively, the ONS-HPCs show high specific capacitance, excellent rate-capability, and outstanding cycling stability under both three-electrode (6 M KOH) and two-electrode (6 M KOH and EMIM BF_4) system. Remarkably, a superior energy density has been achieved when ionic liquid is used as electrolyte. The successful preparation of ONS-HPCs not only turns the low-valued natural biomass derivative into high-valued materials but also provides a great potential advanced electrode material for energy storage device via an awesomely simple, environmental friendly, and low-cost production route.

2. Experimental

2.1 Materials

The kraft lignin, alkaline, was purchased from Wuhan East China Chemical co. LTD, China. The hydrochloric acid was bought from Chengdu Kelon Chemical Reagent Factory, China. Ultrapure water was used throughout the experiments.

2.2 Preparation of lignin-derived 3 D ONS-HPCs

The kraft lignin was directly carbonized in a tubular furnace with temperature firstly increasing from room temperature to 400 °C for 1 h with a heating rate of 2 °C min^{-1}, then followed by a sequentially increasing to the target temperature (600−900 °C) for 1 h with a heating rate of 4 °C min^{-1} under N_2 atmosphere. After the high-temperature treatment, the obtained black solid product was fully grinded and thoroughly washed with 1 mol L^{-1} HCl solution to remove any inorganic salts and further washed with ultrapure water until PH was neutral, and finally dried at 105 °C for 12 h. Depending on the target temperature, the samples are named L-X, where L is the lignin and X means the target temperature. The preparation of each lignin-derived ONS-HPCs sample was repeated three times.

2.3 Materials characterization

The scanning electron microscopy (SEM, JEOL JSM-7001F), transmission electron microscopy (TEM, FEI Tecnai G2 F20), and energy dispersive spectroscopy (EDS) were used to obtain the information about the morphology features and element distribution of samples. The X-ray powder diffraction patterns were recorded by using a PANalytical X'Pert Powder diffractometer with Cu Kα radiation between 5 and 80°. Raman scattering spectra were obtained by Horiba800 Raman spectrometer with wavelength of source laser being 514 nm. The Fourier-

Transform Infrared (FTIR, Thermo Fisher Nicolet iS10) was conducted to get the information about functional groups of kraft lignin. The elemental analyser (EURO EA3000 Elemental Analyzer) and X-ray photoelectron spectroscopy (XPS, Thermo Fisher ESCALAB 250Xi) were carried out to obtain the element content and surface chemical composition of samples. N_2 (77K) adsorption/desorption isotherms were measured with the help of Quantachrome 2SI-MP-9 surface area and pore size analyzer. The specific surface area and pore size distributions of samples were evaluated according to the Brunauer-Emmett-Teller (BET) method and quenched solid density functional theory (QSDFT). The electrical conductivity of the samples were measured by the RTS-9 double electric four-point probe tester.

2.4 Electrochemical measurements

The electrochemical measurements were firstly conducted in a three-electrode system with Hg/HgO as the reference electrode and Pt foil as the counter electrode in 6 M KOH at room temperature. For the preparation of working electrode, the ONS-HPCs, acetylene black, and polytetrafluoroethylene (PTFE) in a weight ratio of 8 : 1 : 1 were well blended in ethanol and then dried in an oven at 80 °C to remove the ethanol. After that, the mixture was rolled into 80−100 μm thickness film and punched into a disk-like film with 12 mm diameter. Followed by dried at 120 °C for 8 h, the electrode was pressed onto nickel foam as current collector. Each working electrode has the area of 1.13 cm^2 with mass loading of 2.5−5.6 mg. To investigate the electrochemical performance of the lignin-based ONS-HPCs as two symmetrical electrodes, a two-electrode configuration was adopted. The CR2032 coin-type symmetric supercapacitors were assembled with two identical lignin-based ONS-HPCs working electrodes separated by cellulose film in 6 M KOH and EMIM BF_4, respectively.

The electrochemical characterization investigation such as cyclic voltammetry (CV), galvanostatic charging−discharging (GCD), and electrochemical impedance spectroscopy (EIS) techniques were conducted on a CHI660E electrochemical working station (Shanghai Chenhua Instrument, Inc., China). The cycling stability was measured by an Arbin MSTAT4 electrochemical workstation. The calculation formulas of specific capacitance (C, F g^{-1}), energy density (E, W h kg^{-1}), and power density (P, W kg^{-1}) are provided in the Supplementary Information.

3. Results and Discussion

3.1 Material characterization

The alkaline kraft lignin, brown color, and its morphology is provide in the Figure S1a. It uniformly contains the carbon, oxygen, and nitrogen elements which mainly come from the kraft lignin itself as well as the sodium, sulphur and the microelements chlorine and potassium that mainly from the impurities such as NaCl, KCl, and $Na_2CO_3 \cdot Na_2SO_4$ which should be recycled from the black liquor but still left in the kraft lignin (Figures S1b-c). Surprisingly, the existed impurities play an important role in the pore generation of hierarchical porous carbons. The schematic illustration of kraft lignin converting into ONS-HPCs is displayed in Figure 1. During the heat-treatment of kraft lignin, the carbonization of kraft lignin produces the char and the Na_2SO_4 can react with the carbon and simultaneously decomposed to form Na_2CO_3 which could act as activation agent and also react with carbon at high-temperature, resulting in the generation of hierarchical pore structure [38]. Meanwhile, the NaCl and KCl can also work as templates to further develop the porous structure in lignin-derived carbon materials. More than that, the produced gases from oxygen-containing functional groups of kraft lignin (Figure S1d and Table S1) under high-temperature such as H_2O and CO_2 which are well known activating agents for carbons probably induce a substantial co-activation for the carbon materials and further promote the generation of pores [19, 21, 42].

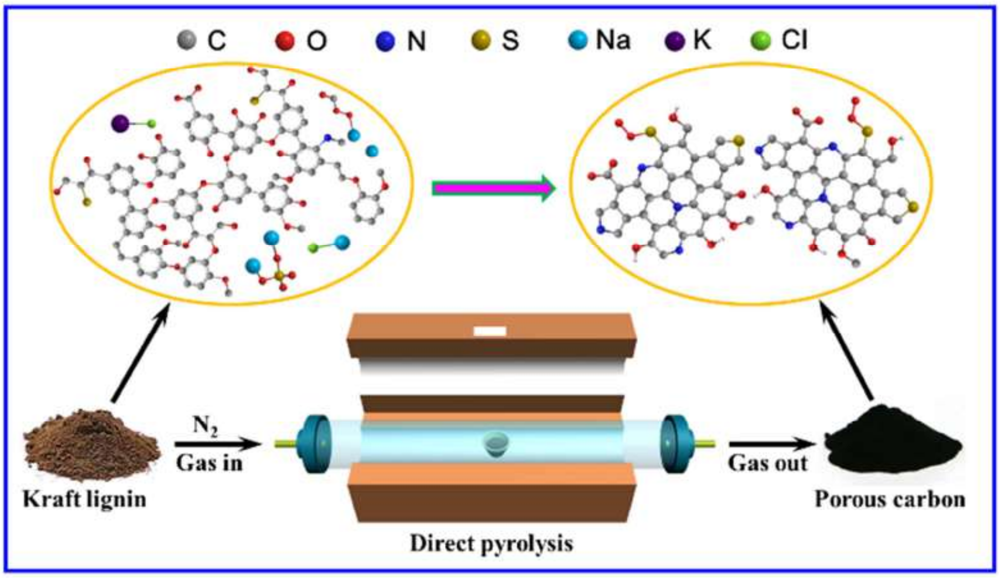

Figure 1. Schematic illustration of the direct conversion of kraft lignin into the O-N-S co-doped hierarchical porous carbons (ONS-HPCs).

As shown in Figures 2a−d, all lignin-derived ONS-HPCs samples exhibit three-dimensional frameworks with numerous interconnected macropores and thin pore walls. Furthermore, the oxygen, nitrogen and sulfur elements are successfully and uniformly doped into the entire carbon structure, as reflected by the elemental mappings images of L-700 (Figures 2e−h). In addition to macropores, the Transmission Electron Microscopy (TEM) and high-resolution TEM (HRTEM) images indicate that all ONS-HPCs samples possess the some cross-link mesopores ranging from about 20−50 nm (Figures 2i−l) and plentiful micropores with sizes less than 2 nm (Figures 2m−p) within the sheet-like microstructure. The opened 3D hierarchical porous structures contain macropores, mesopores, and micropores, being highly conductive to the ions fast transfer and diffusion and thus enhance the electrochemical performance. In addition, the HRTEM analysis of L-900 shows that the typical sheet contains not only amorphous carbon structure but also the range-ordered graphitic region featuring with obvious lattice fringes with lattice spacing of 0.35 nm, in agreement with the *d*-spacing of (002) plane of graphitic carbon [43]. The formation of graphitic region is favorable for the electrical conductivity of L-900, as demonstrated by the measured highest electrical conductivity of 33.3 S m^{-1} of L-900 in Table S3.

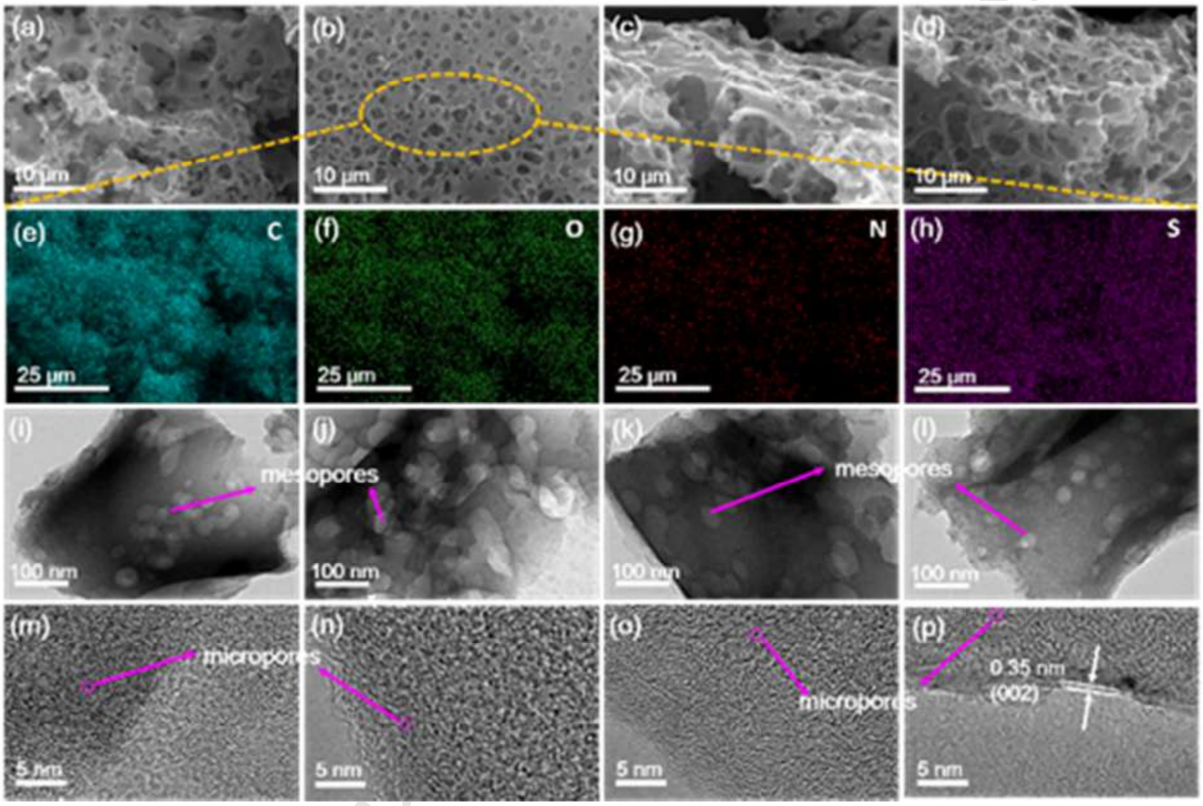

Figure 2. The microstructure characterization of the as-prepared three-dimensional ONS-HPCs: SEM images of the ONS-HPCs obtained at (a) 600, (b) 700, (c) 800, and (d) 900 °C; the (e-h) EDS elemental mappings of L-700; TEM and HRTEM images of (i, m) L-600, (j, n) L-700, (k, o), L-800, and (l, p) L-900.

The structure characteristics of the ONS-HPCs samples were also further determined by X-ray diffraction (XRD) and Raman spectroscopy. Two broad peaks (002) and (100) located approximately at 22.6° and 43.5° are observed for L-600, L-700, L-800, and L-900 in Figure 3a, implying their amorphous carbon structure. However, the diffraction peak of graphite located at 26.4º starts to emerge when the temperature elevates to 900 ºC, implying the partial graphitized of L-900, which is agreement with the result of HRTEM. In addition, a large enhancement in the intensity of small-angle region of L-700, L-800 and L-900 is also observed, indicative of the presence of plentiful micropores [13, 44, 45]. The Raman spectra of all ONS-HPCs samples are displayed in Figure 3b. All the samples exhibit two distinct bands 1350 and 1595 cm^{-1}, corresponding to D band rising from defects and disorder of carbon material and the G band associated with the ordered graphite sp^2 C−C bond in-plane vibrations, respectively [5]. The intensity ratio I_D/I_G is regarded as the indicator of the structural defects of carbon materials, and a smaller value suggests less defects and higher degree of graphitization in carbon materials. The intensity ratio I_D/I_G calculated according to the integrated areas of the D-band and G-band (Figure. S2) are to be 3.15, 2.88, 2.67, and 2.39 for L-600, L-700, L-800 and L-900, respectively. Obviously, the intensity ratio I_D/I_G decreases with the temperature increasing, implying the gradually deceased structural defects and more graphitic structure in these carbon materials.

The pore structure properties of the ONS-HPCs samples were studied by N_2 adsorption-desorption measurements (Figures 3c-d). All curves exhibit the typical IV type isotherms according to the IUPAC classification. The steep N_2 uptake at $P/P_0 < 0.2$, a hysteresis loop at P/P_0 in the range of 0.45−0.9, and the sudden enhancement at $P/P_0 > 0.9$ can be observed, demonstrating the co-existence of micropores, mesopores, and macropores in these samples. These results are consistent with electron microscope analysis, namely, all lignin-derived carbon materials possess the hierarchical pore structure with the coexistence of micropores, mesopores, and macropores. Furthermore, the pore size distribution in Figure 3d presents that the micropores with size ranging from 0.61 to 2.0 nm account for the larger part of the pore volume than the mesopores ranging from 2.0–5.0 nm in these samples. The specific surface area (SSA) (Table S2) is only 338 m^2 g^{-1} for L-600, and dramatically enhanced from 1269 m^2 g^{-1} (L-700) to a highest value of 1307 m^2 g^{-1} (L-800), but abruptly dropped to 1084 m^2 g^{-1} when the HPCs are prepared at 900 ºC. The decrease of SSA at 900 ºC is attributed to that the higher temperature merges and reconstructs some micropores and mesopores, collapses some small branches, resulting in the decrease of SSA. The change trend of pore volume is similar to the SSA (Table S2). For an ideal electrode material, such a hierarchical porous structure with large SSA is desirable, since the high SSA could provide lots of active sites for the formation of double electrode layer and the hierarchical porous structure possesses the macropores that served as ion-buffering accommodation can supply electrolyte ion, and mesopores acted as ion-highways that minimize ion-diffusion distance during the quick charging/discharging process, ensuring the high rate performance and power density, and the ample micropores that endow a large ion-accessible surface area for charge reservoirs, guaranteeing the large specific capacitance and energy density.

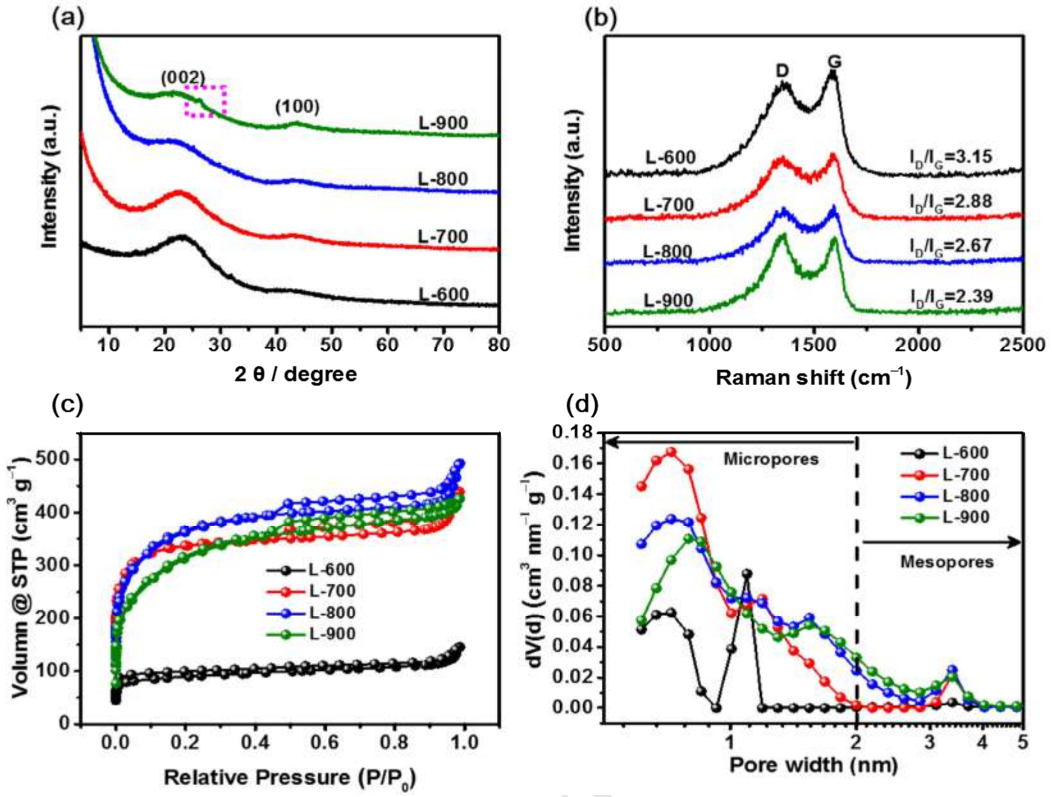

Figure 3. The structure and porosity characterizations of the as-prepared three-dimensional ONS-HPCs: (a) XRD patterns, (b) Raman spectra, (c) N_2 adsorption-desorption isotherms, and (d) pore size distribution curves determined by QSDFT of L-600, L-700, L-800, and L-900.

The element contents of lignin-derived ONS-HPCs samples are listed in Table S2. The carbon, oxygen, nitrogen, and sulfur contents of these samples are 80.13−90.1%, 5.63−13.21%, 1.91−3.98%, and 0.96−2.72%, respectively. Notably, the total contents of the functionalized heteroatoms doped in ONS-HPCs decrease from 19.91% to 9.84 %with elevating the pyrolysis temperature from 600 ºC to 900 ºC (Table S2). Among them, the oxygen and nitrogen contents decrease along with the pyrolysis temperature increasing since the oxygen and nitrogen-containing functionalities are unstable and decomposed under higher temperature. As for sulfur element, its content firstly decreases with temperature gradually increasing to 800 ºC but then suddenly increases when temperature rises to 900 ºC, resulting in the higher sulfur content of L-900 than that of L-700 and L-800. This is attributed to that the sulfur-containing functional groups in kraft lignin undergo the thermochemical sulfate reduction and thermal decomposition of sulfides under high temperature, leading to the formation of H_2S [46, 47]. The H_2S decomposes into hydrogen and sulfur when temperature ≥ 800 ºC, then the sulfur reacts with carbon to form C-S [48]. However, the H_2S conversion at 800 ºC is extremely low which can be ignored, while the conversion remarkably increases when temperature is 900 ºC [48]. Thus, more sulfur forms at 900 ºC and reacts with carbon, resulting in the sulfur element retained in the L-900. The surface chemical components of the kraft lignin and its derived ONS-HPCs samples were characterized by X-ray photoelectron spectroscopy (XPS) and the obtained element contents are also summarized in Table S2. As shown in Figure 4a, the kraft lignin contains many elements mainly concentrating on carbon, oxygen, nitrogen, sulfur, and sodium elements (microelements chlorine and potassium are not obvious). The elements like sodium, potassium, and chlorine are eliminated during the washing process, while the oxygen, nitrogen, and sulfur are doped into the carbon skeleton of ONS-HPCs. And these heteroatoms content detected by XPS shows similar change rule with those measured by elemental analyzer. To figure out the detailed chemical states of the doped-heteroatoms in ONS-HPCs, the high resolution XPS spectrum of each element is necessary. As exhibits in Figures 4b and S3, the high resolution of C 1s XPS spectra could be fitted into five individual peaks located at around 283.6−283.8, 284.7, 285.6−285.9, 288.0−288.4, and 290.1−291.1 eV, corresponding to the C-S, C-C/C=C, C-N/C-O, O-C=O, and COOR binding, respectively **[20, 49, 50]**. The O 1s spectra (Figures 4c and S3) could be further resolved into four different peaks, which clearly reveals the existence of oxygen-containing functional groups including C=O (530.4−530.6 eV), C-OH and/or C-O-C

(531.5−532.1 eV), O=C-O (532.8−533.6 eV), and chemisorbed oxygen (O=C-OH carboxylic groups) or absorbed water (535.0−535.5 eV) **[7, 49, 51]**. The N 1s spectra (Figures 4d and S3) was deconvoluted into four peaks with binding energies centered at around 398.2−398.6, 399.1−400.1, 401.2−401.7, and 402.8−403.1 eV, assigning to pyridinic-N (N-6), pyrrolic and/or pyridonic-N (N-5), quaternary-N (N-Q), and oxidized-N (N-X), respectively **[52-54]**. As pyrolysis temperature increases to 900 ºC, the N 1s high-resolution spectrum only could be fitted into two peaks, assigning to N-5 and N-Q (Figure S3). In the S 2p XPS spectra (Figures 4e and S3), three deconvoluted peaks are obtained, revealing the presence of C-S bond located at 163.2−164.0 and 164.3−165.2 eV and the oxidized sulfur moieties (-SO_n-) centered at around 167.8−168.7eV **[20, 55]**. Accordingly, based on the above results, the possible locations of N, O, and S-containing functional groups on the carbon network is presented in Figure 4f. These doped heteroatoms could enhance the wettability and electrochemical activity of the ONS-HPCs as well as providing extra pseudocapacitance contribution [26, 56]. These results definitively demonstrate that the natural biomass derivative kraft lignin have been successfully converted into functionalized HPCs with O-N-S co-doping. Owing to the distinctive features such as hierarchical pore structure, high specific area, high-level heteroatom doping, and 3D framework, it is expected that these carbon materials could have a great potential in electrode materials.

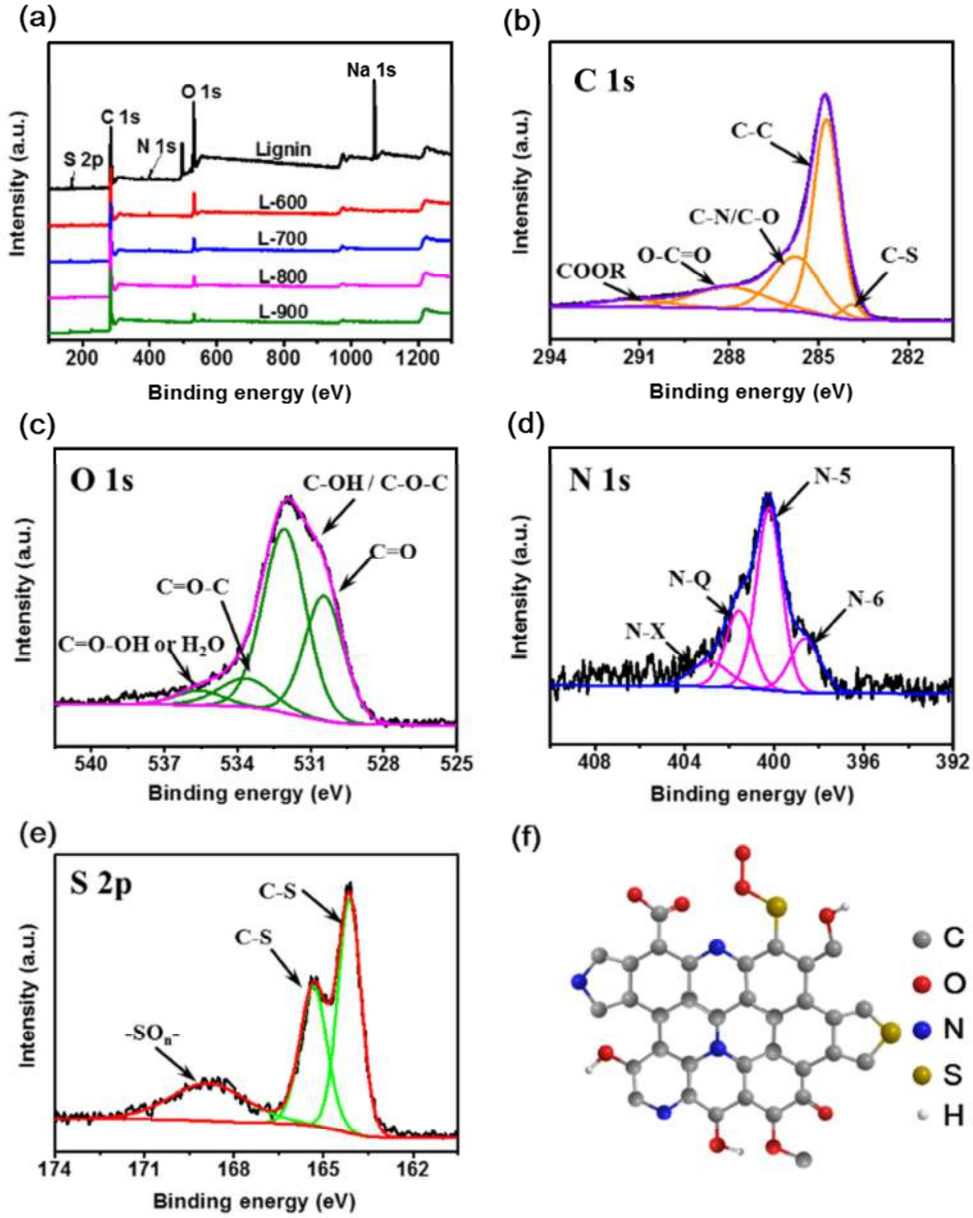

Figure 4. Surface composition analysis of as-prepared ONS-HPCs: (a) XPS survey spectra of the kraft lignin and ONS-HPCs obtained at different temperatures; the high-resolution of (b) C 1s, (c) O 1s, (d) N 1s, and (e) S 2p XPS spectra of L-700; (f) Possible locations for heteroatoms O, N, and S incorporation into the carbon skeleton.

3.2 Electrochemical performance

The in-depth insight into the electrochemical properties of as-prepared lignin-derived ONS-HPCs is necessary to exploit their electrochemical applications. As shown in Figure 5a, the cyclic voltammetry (CV) curves of L-600, L-700, L-800, and L-900 at the scan rate of 10 mV s^{-1} in 6 M KOH aqueous electrolyte obviously present a mildly distorted rectangular CV curves with a broad hump, revealing the capacitive performance accompanied by pseudocapacitance characteristics attributed to the existence of heteroatoms-containing functional groups **[45, 56]**. Especially, this hump gradually weakens with the increase of pyrolysis temperature, ascribing to the decreased number of heteroatoms. Obviously, the CV curve closed area of L-700 is the largest, indicative of its highest gravimetric specific capacitance, even though that the L-700 does not possess the largest specific surface area or the most doping-heteroatoms (Table S2). This result should be originated from the optimum synergistic effect between electric double-layer capacitor of specific surface area and faradaic pseudocapacitance of heteroatoms-containing functional groups, making L-700 possess the highest specific capacitance. The CV curves of these four carbon samples at different scan rates are provided in Figure S4. It can be seen that CV curve of L-700 still maintains the similar rectangular profile at 200 mV s^{-1}, indicating its superior rate capability. As for the carbon materials obtained at higher temperature, the CV curves of L-800 and L-900 show the rectangular-like shape with minor deviation even at a larger scan rate of 400 mV s^{-1}, suggesting that higher temperature is beneficial for enhancing the rate handling ability of carbon materials with improved electric conductivity. Besides, all galvanostatic charging−discharging (GCD) profiles of the ONS-HPCs samples at 0.5 A g^{-1} exhibit imperfectly symmetrical triangular shape with non-linear characteristics, attributing to the Faradic reaction induced by heteroatoms-containing functional groups (Figure 5b). Furthermore, the L-700 electrode presents the highest specific capacitance of 300.5 F g^{-1} at 0.5

A g^{-1}, which is much higher than 252 F g^{-1} of L-600, 243.6 F g^{-1} of L-800, and 184 F g^{-1} of L-900 (Figure 5c). Notably, even at an ultrahigh current density of 60 A g^{-1}, the specific capacitance of L-700 still can be achieved as high as 243 F g^{-1} with 80.9 % retention of initial capacitance (the detailed calculations based on Figure S5), further implying its excellent rate property. As exhibited in Figure 5d, the L-700 electrode still retains 95.5% of its initial capacitance at the current density of 10 A g^{-1} after 10000 cycles, indicating the outstanding electrochemical durability. Strikingly, such the high electrochemical performance of L-700 is superior to or comparable to that of previously reported lignin-derived or other biomass-based carbon materials even prepared with additional activating agents (Table S4).

Furthermore, the electrochemical impedance spectroscopy (EIS) measurement with a frequency of 100 kHz to 0.01 Hz was carried out to investigate the resistance and capacitive behavior of the as-prepared ONS-HPCs. As shown in Figure 5e, the Nyquist plots of the four samples exhibit the nearly vertical line at low frequencies, implying the nearly ideal capacitive performance. Among them, L-700 electrode has the steepest line, indicating the best capacitive behavior in the low frequency region. The ESR values of the L-600, L- 700, L-800, and L-900 are 0.44, 0.45, 0.51, and 0.56 Ω, respectively. Except L-600, the semi-circle diameters of L-700, L-800, and L-900 are very small, meaning the low charge transfer resistance of these three carbon materials. From the bode phase diagrams (Figure 5f), the phase angle of L-700 is ~83.5º, closely to an ideal capacitor with phase angle of 90º, which is also larger than 80.5º of L-600, 81.4º of L-800, and 80.3º of L-900, further demonstrating the best capacitive performance of L-700. The relaxation time constants τ_0 that determined by $\tau_0 = 1/f_0$ at a phase angle of -45º can be used to evaluate how fast an electrode can be discharged [57]. The L-900 has a τ_0 value of 1.58 s, smaller than 5.85 s of L-600, 3.12 s of L-700, and 1.82 s of L-800, implying that L-900 is able to achieve the best rate capability at larger charge–discharge current density. Apparently, owing to their relatively low ion-diffusion resistance, ESR, R_{ct} and excellent capacitive performance, the L-700, L-800, and L-900 are more accessible for the achievement of high electrochemical performance.

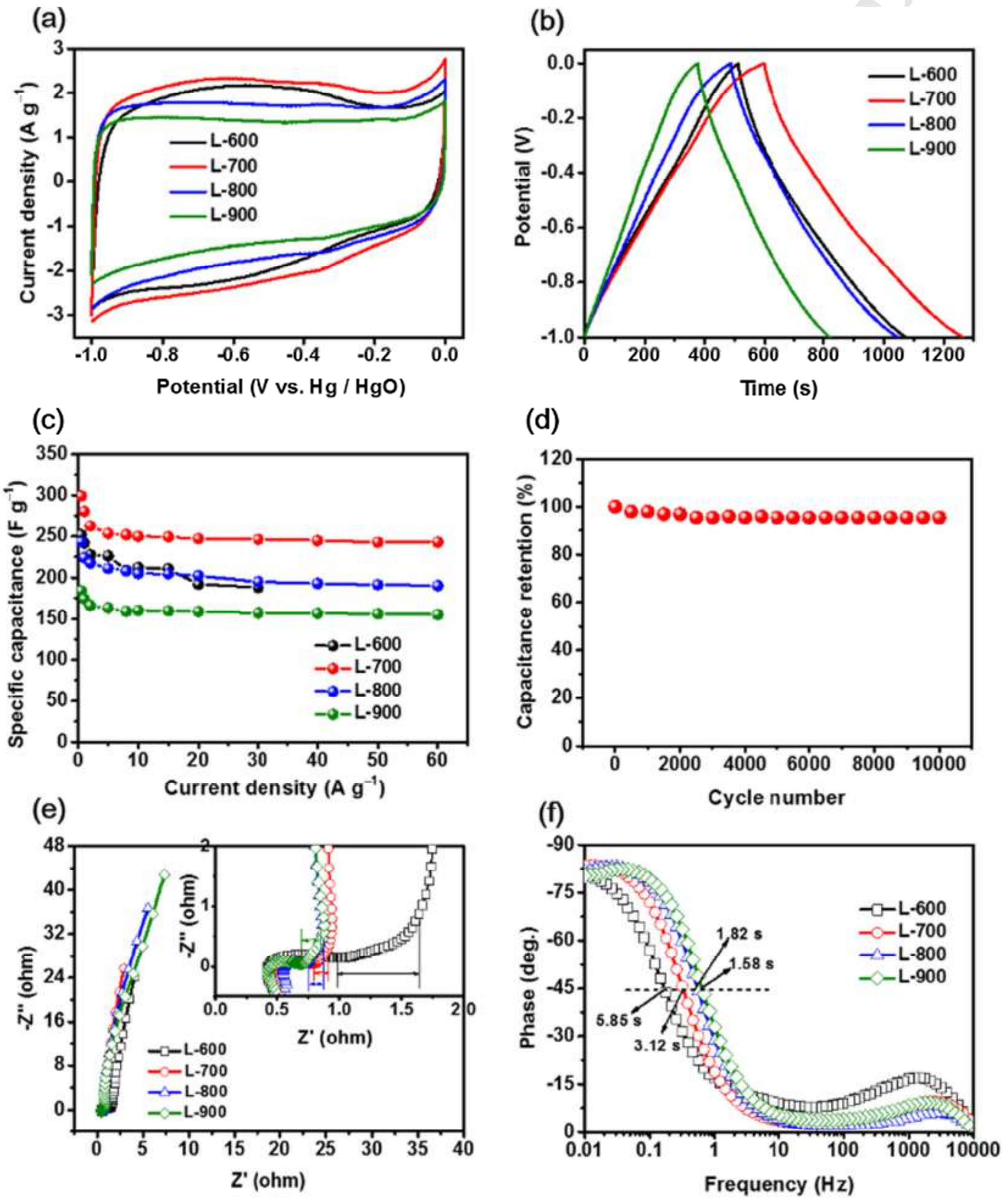

Figure 5. Electrochemical performances of the lignin-derived ONS-HPCs samples measured in a three-electrode system in 6 M KOH: (a) CV curves at the scan rate of 10 mV s^{-1}; (b) GCD profiles at the current density of 0.5 A g^{-1}; (c) specific capacitances *versus* current densities; (d) cycling performance of the L-700 at 10 A g^{-1}; (e) the Nyquist plots and (f) the bode phase diagrams of the ONS-HPCs samples.

Due to the superior electrochemical performance of the lignin-derived ONS-HPCs in three-electrode, it is necessary to investigate their practical performance. Hence, the symmetric supercapacitors were assembled with two identical ONS-HPCs-based electrodes in 6 M KOH aqueous electrolyte. The CV and GCD curves of the ONS-HPCs based symmetric supercapacitors except the L-600 based supercapacitors show the rectangle-like and approximate isosceles triangle shapes even at a rather high scan rate and current density, implying their predominant electric double-layer capacitor behavior and excellent rate performance (Figures. 6a, b and S6). The L-700//L-700 symmetric supercapacitor has none of the unpredictability of the largest current response and closed area, indicative of its highest specific capacitance (Figure 6c). The specific capacitance of L-700-based supercapacitor is 244.5 F g^{-1} at 0.2 A g^{-1} and still maintains 200 F g^{-1} even at a high current density of 40.0 A g^{-1}, with 81.8% retention of its initial capacitance, suggesting the ultrahigh rate capability (Figure 6d). Furthermore, the specific capacitance of L-700//L-700 symmetric supercapacitor is better than that of previously reported symmetric supercapacitors assembled with the lignin-derived or other natural biomass-based carbon materials, as listed in Table S5. After 10000 cycles at 5.0 A g^{-1}, this device only presents 8.4% capacitance decay in comparison with its initial value, revealing the outstanding cycling performance (Figure 6e). The Ragone plot shows that the L-700//L-700 symmetric supercapacitor delivers a maximum energy density of 8.5 W h kg^{-1} at a power density of 100 W kg^{-1}. Surprisingly, the energy density of 4.6 W h kg^{-1} is still maintained even at the high power density of 16.4 kW kg^{-1} (Figure 6f). Such excellent output performance is better than that of many biomass-derived carbon-based symmetric supercapacitors previously reported [51, 57-61]. The results demonstrates that the L-700 based symmetric supercapacitor can deliver high energy density with less sacrificing the power density in 6 M KOH.

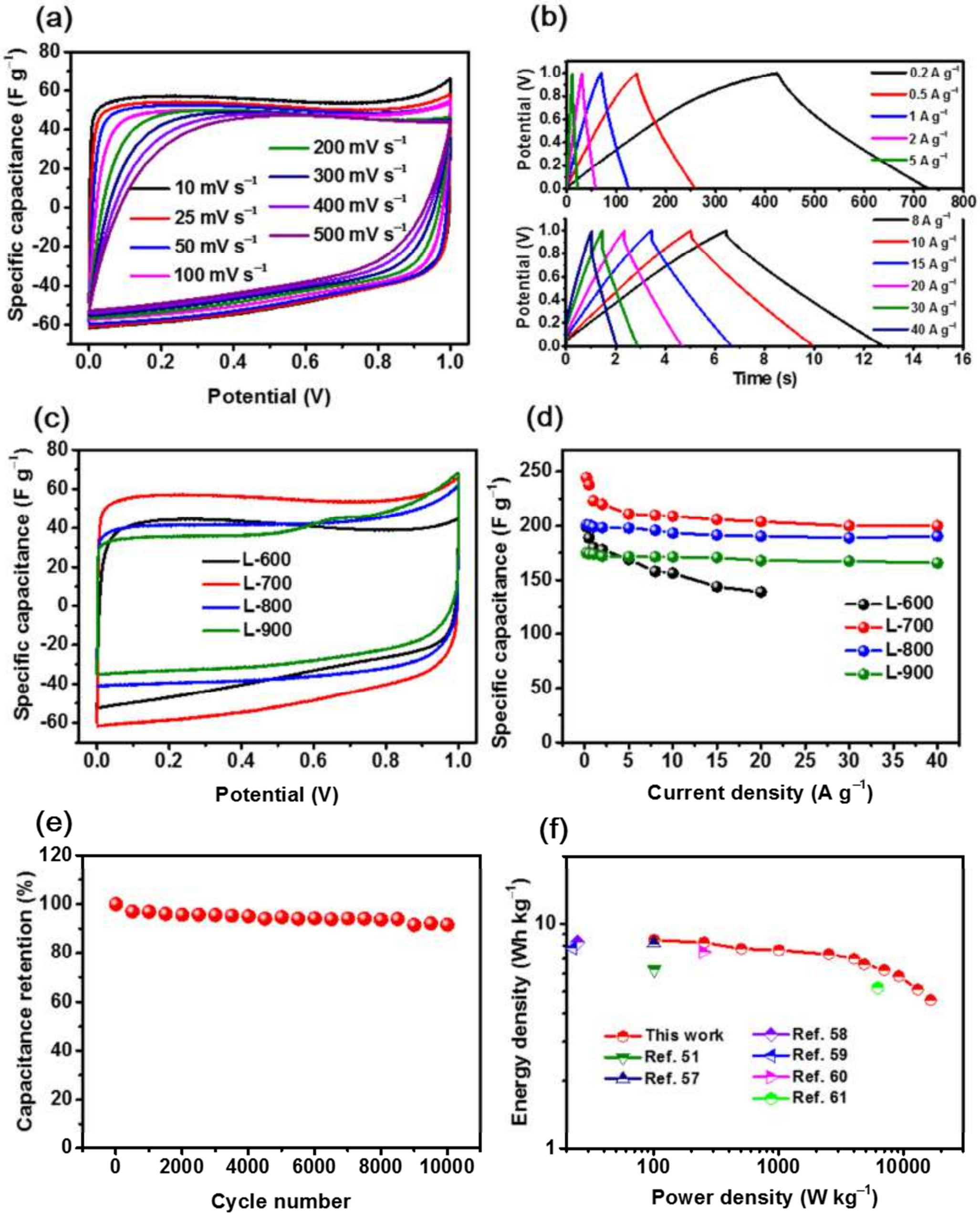

Figure 6. Electrochemical performances of the ONS-HPCs-based electrodes in a two-electrode system in 6 M KOH: (a) CV curves of L-700 based supercapacitor; (b) GCD profiles of L-700 based supercapacitor; (c) A comparison of the CV curves at 10 mV s^{-1}; (d) the specific capacitances calculated at different current densities; (e) the cycling performance and (f) the Ragone plot of the L-700 based supercapacitor.

Except for aqueous electrolyte, the ionic liquid EMIM BF_4 electrolyte which is conductive to obtain high operating voltage and enhance energy density was employed to test and verify the energy storage applications of ONS-HPCs. We selectively used three samples (L-700, L-800, and L-900) to develop the ONS-HPCs-based symmetric supercapacitors in EMIM BF_4. Their CV curves at 50 mV s^{-1} and GCD profiles at 1.0 A g^{-1} are shown in Figures. 7a and b. Interestingly, unlike in 6 M KOH aqueous electrolyte, it is the L-900 has the largest closed area and longest discharge time, demonstrating the best specific capacitance of L-900. In addition, compared with the L-700 and L-800 based supercapacitors, the CV curve of L-900 based symmetric supercapacitors at scan rate of 500 mV s^{-1} still maintains the similar shape with that at small scan rates, revealing the fast ion transportation in the highly interconnected structure and excellent rate performance (Figure S7). The specific capacitances of these ONS-HPCs calculated based on the GCD profiles (Figure S7) are shown in Figure 7c. The L-900 shows a high gravimetric specifc capacitance of 157 F g^{-1} at 1.0 A g^{-1}, higher than not only 134 F g^{-1} of L-700 and 148 F g^{-1} of L-800 but also that of many reported biomass-derived carbon-based supercapacitors (Table S5). Impressively, the L-900 based supercapacitor still holds the specific capacitance of 130.0 F g^{-1} at 30 A g^{-1} with 82.8% retention, and its excellent rate capability is much better than that of L-700 (54.7 % retention) and L-800 (63.0 % retention) based supercapacitors. The better electrochemical performance of L-900 based supercapacitor could be probably explained by its higher efficient use of specific surface area and better electron conductivity from partical graphitized region of L-900. The pore sizes (i.e., average pore width) of L-700 and L-800 are both 0.723 nm which is smaller than $EMIM^+$ size (0.79 nm of $EMIM^+$ and 0.48 nm of BF_4^-) [62, 63], leading to a limited accessibility of these small pores to the large cations and then the decrease of specific capacitance [62]. While the pore size of L-900 is 0.795 nm that being close to the ion size, this larger size can make the electrolyte ions be able to be adsorbed into the inside pores and adequately access the pore surface without constraints which is beneficial to make the full use of the specific surface area and then increase the electrochemical performance of carbon materials [64] and larger pore size decreases the ionic resistance and produces a more capacitive behaviour [65]. Furthermore, the pore volumes of the L-700, L-800 and L-900 are 0.598, 0.668, and 0.610 $cm^3\ g^{-1}$ respectively (Table S2) and the ratios of pores lower than 0.79 nm for L-700, L-800 and L-900 are 38.67, 28.0, and 20.6% respectively, meaning that more small free space of L-700 and L-800 can’t be effectively accessible for large cations in comparison with L-900. More than that, compared with L-700 and L-800, the defunctionalized surface of L-900 makes it equally favourable for $EMIM^+$ and BF_4^- to shuttle back and forth in pores [65]. In addition to these, the outstanding electron conductivity of L-900 with partial graphitized structure can improve the rate performance. But compared with in KOH aqueous solution, the ONS-HPCs-based supercapacitors in EMIM BF_4 display the relative low specific capacitance which could be probably attributed to the large ion size, high viscosity and low ion conductivity of EMIM BF_4 (15.5 mS cm^{-1} of EMIM BF_4 *vs.* 600 mS cm^{-1} of KOH aqueous solution) [11, 66]. After 10000 cycles at 5 A g^{-1}, the L-900 based symmetric supercapacitor still retains 88.5% of its initial capacitance, presenting its excellent cycling ability (Figure. 7d). The Ragone plot (Figure. 7e) presents that the L-900 based supercapacitor possesses a high energy density of 66.8 W h kg^{-1} at a power density of 1.75 kW kg^{-1}, and still maintains 32.2 W h kg^{-1} even at an ultrahigh power density of 40.0 kW kg^{-1}, which is much better than that of reported carbon-based supercapacitors [24, 57, 67-71]. To examine its practical prospects, as shown in Figure.7f, an as-fabricated CR2032 coin-type L-900 based symmetric supercapacitor can light up lots of 3 V green LEDs. Therefore, this work suggestes the large potential of lignin-derived ONS-HPCs as advanced electrode materials for promising energy-storage devices.

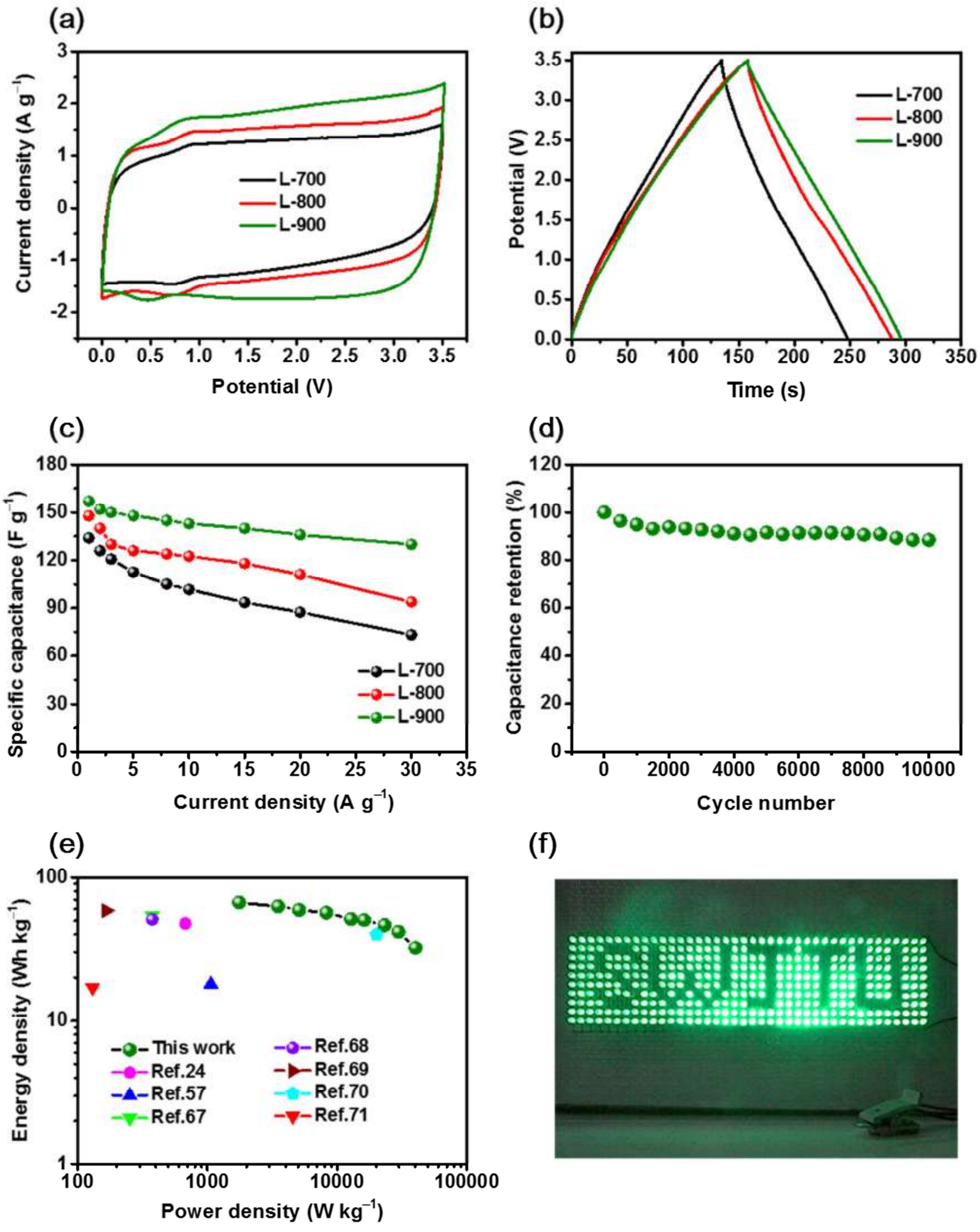

Figure 7. Electrochemical performances of ONS-HPCs-based symmetric supercapacitors in EMIM BF_4: (a) A comparison of the CV curves at 50 mV s^{-1}; (b) GCD profiles at 1.0 A g^{-1}; (c) the specific capacitances calculated at different current densities of L-700, L-800, and L-900

based supercapacitors; (d) the long-term cycle ability of L-900 based supercapacitor; (e) the Ragone plot of the L-900 based supercapacitor; and (f) photograph of green LEDs lit by one L-900 based device.

Such excellent electrochemical performance of the lignin-derived ONS-HPCs samples with high specific capacitance, excellent rate capability and remarkable cycling durability should be mainly ascribed to the following reasons: (i) the raw material alkaline kraft lignin with uniform distribution of self-doping elements provides a superior base for the production of desirable carbon materials; (ii) the abundant micro-, meso-, and macropores in the hierarchical porous structure with high surface area can provide not only lots of charge accumulation for the high capacitance but also the ion channels for the effective ion rapidly-shuttling back and forth; (iii) the 3 D interconnected skeleton with excellent electron conductivity benefits the electron pathways, greatly enhancing the rate capability; (iv) the abundant heteroatoms (N, O, and S) incorporation effectively improves the hydrophilia of the ONS-HPCs and provides the extra pseudocapacitance via redox reactions; and (v) the synergistic effect between pore structure and doped heteroatoms could make the as-obtained ONS-HPCs exploit their advantages to the full in different electrolytes. Therefore, this work fully demonstrates the large potential of natural biomass-derived ONS-HPCs for promising energy-storage devices and also enlightens us that it can easily realize the large-scaled production of the sustainable carbon materials for high-performance energy conversion and storage devices via a rather simple, green-environmentally, and low-budget approach.

4. Conclusions

In this work, we employed an environmentally friendly, extremely simple, and low-cost self-activation process to successfully prepare the O, N, and S co-doped hierarchical porous carbons (ONS-HPCs) by direct pyrolysis of the natural biomass derivative kraft lignin, the byproduct from papermaking black liquor. The impurities existed in kraft ligin such as NaCl, KCl and $Na_2CO_3 \cdot Na_2SO_4$ and the pyrolysis gases play an important role in the generation of ONS-HPCs. The 3 D highly interconnected ONS-HPCs feature high specific surface areas (338−1307 m^2 g^{-1}) with abundant macro-, meso- and micropores and plentiful oxygen, nitrogen, and sulfur uniform doping (9.84−19.91 wt%). When assembled into a symmetric supercapacitor in 6 M KOH, the ONS-HPCs-based electrode delivers a high specific capacitance of 244.5 F g^{-1} at 0.2 A g^{-1}, excellent rate capability of remaining 81.8% of initial value even at 40.0 A g^{-1} and superior cycling performance with only 8.4% capacitance decay after 10000 cycles. The device delivers a high energy density of 8.5 W h kg^{-1} at a power density of 100 W kg^{-1}. Significantly, the energy density increases to 66.8 W h kg^{-1} at a power density of 1.75 kW kg^{-1} when EMIM BF_4 works as electroyte in device, and still holds 32.2 W h kg^{-1} even at an ultrahigh power density of 40.0 kW kg^{-1}, which is much better than that of many reported carbon-based supercapacitors. This work fully demonstrates the successful conversion of the natural biomass derivative kraft lignin into the sustainable and high-performance electrode materials via a green and simple way and also develops a valuable utilization way for kraft lignin and a good raw material for the high-performance electrode material. But, it still needs further research and endeavour to explore the large-scaled electrode production for high-performance energy conversion and storage devices and to prepare preferable electrode material from the kraft lignin via a simple, green-environmentally and low-budget approach.

Acknowledgments

This work was supported by the Scientific and Technological Projects for International Cooperation of Sichuan Province (No. 2017HH0069), the Independent Research Project of State Key Laboratory of Traction Power (No. 2016TPL_Z03 and No. 2017TPL_Z04), and the Fundamental Research Funds for the Central Universities of China (Nos. 2682016CX074, 2682017CY06, 2682016ZY01, and 2682017ZDPY01).

References

[1] Li H, Yuan D, Tang C, Wang S, Sun J, Li Z, et al. Lignin-derived Interconnected Hierarchical Porous Carbon Monolith with Large Areal/volumetric Capacitances for Supercapacitor. Carbon 2016;100:151-7.

[2] Zhang Y, Liu X, Wang S, Li L, Dou S. Bio-Nanotechnology in High-Performance Supercapacitors. Adv Energy Mater 2017;7:1700592.

[3] Zhao J, Jiang Y, Fan H, Liu M, Zhuo O, Wang X, et al. Porous 3D Few-Layer Graphene-like Carbon for Ultrahigh-Power Supercapacitors with Well-Defined Structure-Performance Relationship. Adv Mater 2017;29:1604569.

[4] Zhai Y, Dou Y, Zhao D, Fulvio PF, Mayes RT, Dai S. Carbon Materials for Chemical Capacitive Energy Storage. Adv Mater 2011;23:4828-50.

[5] Yu P, Zhang Z, Zheng L, Teng F, Hu L, Fang X. A Novel Sustainable Flour Derived Hierarchical Nitrogen-Doped Porous Carbon/Polyaniline Electrode for Advanced Asymmetric Supercapacitors. Adv Energy Mater 2016;6:1601111.

[6] Gao F, Shao G, Qu J, Lv S, Li Y, Wu M. Tailoring of Porous and Nitrogen-rich Carbons Derived from Hydrochar for High-performance Supercapacitor Electrodes. Electrochim Acta 2015;155:201-8.

[7] Li L, Liu E, Li J, Yang Y, Shen H, Huang Z, et al. A Doped Activated Carbon Prepared from Polyaniline for High Performance Supercapacitors. J Power Sources 2010;195:1516-21.

[8] Zuo S, Chen J, Liu W, Li X, Kong Y, Yao C, et al. Preparation of 3D Interconnected Hierarchical Porous N-doped Carbon Nanotubes. Carbon 2018;129:199-206.

[9] Hao P, Zhao Z, Tian J, Li H, Sang Y, Yu G, et al. Hierarchical Porous Carbon Aerogel Derived from Bagasse for High Performance Supercapacitor Electrode. Nanoscale 2014;6:12120-9.

[10] Zhang F, Lu Y, Yang X, Zhang L, Zhang T, Leng K, et al. A Flexible and High-voltage Internal Tandem Supercapacitor Based on Graphene-based Porous Materials with Ultrahigh Energy Density. Small 2014;10(11):2285-92.

[11] Wang YG, Song YF, Xia Y. Electrochemical Capacitors: Mechanism, Materials, Systems, Characterization and Applications. Chem Soc Rev 2016;45:5925-50.

[12] Dutta S, Bhaumik A, Wu KC-W. Hierarchically Porous Carbon Derived from Polymers and Biomass: Effect of Interconnected Pores on Energy Applications. Energ Environ Sci 2014;7:3574-92.

[13] Hou J, Jiang K, Wei R, Tahir M, Wu X, Shen M, et al. Popcorn-Derived Porous Carbon Flakes with an Ultrahigh Specific Surface Area for Superior Performance Supercapacitors. ACS Appl Mater Interfaces 2017;9:30626-34.

[14] Lin T, Chen W, Liu F, Yang C, Bi H, Xu F, et al. Nitrogen-doped Mesoporous Carbon of Extraordinary Capacitance for Electrochemical Energy Storage. Science 2015;350(6267):1508-13.

[15] Gutiérrez MC, Jobbágy M, Rapún N, Ferrer ML, del Monte F. A Biocompatible Bottom-Up Route for the Preparation of Hierarchical Biohybrid Materials. Adv Mater 2006;18:1137-40.

[16] Estevez L, Dua R, Bhandari N, Ramanujapuram A, Wang P, Giannelis EP. A Facile Approach for the Synthesis of Monolithic Hierarchical Porous Carbons – High Performance Materials for Amine Based CO_2 Capture and Supercapacitor Electrode. Energ Environ Sci 2013;6:1785-90.

[17] Chen CJ, Zhang Y, Li YJ, Dai JQ, Song JW, Yao YG, et al. All-wood, Low Tortuosity, Aqueous, Biodegradable Supercapacitors with Ultra-high Capacitance. Energ Environ Sci 2017;10:538-45.

[18] Mohan D, Jr. CUP. Activated Carbons and Low Cost Adsorbents for Remediation of Tri- and Hexavalent Chromium from Water. J Hazard Mater 2006;137:762-811.

[19] Xia C, Shi SQ. Self-activation for Activated Carbon from Biomass: Theory and Parameters. Green Chem 2016;18:2063-71.

[20] Zhao G, Chen C, Yu D, Sun L, Yang C, Zhang H, et al. One-Step Production of O-N-S Co-Doped Three-Dimensional Hierarchical Porous Carbons for High-Performance Supercapacitors. Nano Energy 2018;47:547-55.

[21] Fierro V, Torné-Fernández V, Celzard A. Methodical study of the chemical activation of Kraft lignin with KOH and NaOH. Microporous Mesoporous Mater 2007;101(3):419-31.

[22] Gonzalez-Serrano E, Cordero T, Rodriguez-Mirasol J, Cotoruelo L, Rodriguez JJ. Removal of water pollutants with activated carbons prepared from H_3PO_4 activation of lignin from kraft black liquors. Water Res 2004;38(13):3043-50.

[23] Fierro V, Torné-Fernández V, Celzard A. Kraft lignin as a precursor for microporous activated carbons prepared by impregnation with ortho-phosphoric acid: Synthesis and textural characterisation. Microporous Mesoporous Mater 2006;92:243-50.

[24] Wang D, Liu S, Fang G, Geng G, Ma J. From Trash to Treasure: Direct Transformation of Onion Husks into Three-Dimensional Interconnected Porous Carbon Frameworks for High-Performance Supercapacitors in Organic Electrolyte. Electrochim Acta 2016;216:405-11.

[25] Ma Z, Zhang H, Yang Z, Ji G, Yu B, Liu X, et al. Mesoporous Nitrogen-doped Carbons with High Nitrogen Contents and Ultrahigh Surface Areas: Synthesis and Applications in Catalysis. Green Chem 2016;18:1976-82.

[26] Li Y, Wang G, Wei T, Fan Z, Yan P. Nitrogen and Sulfur Co-doped Porous Carbon Nanosheets Derived from Willow Catkin for Supercapacitors. Nano Energy 2016;19:165-75.

[27] Nasini UB, Bairi VG, Ramasahayam SK, Bourdo SE, Viswanathan T, Shaikh AU. Phosphorous and Nitrogen Dual Heteroatom Doped Mesoporous Carbon Synthesized via Microwave Method for Supercapacitor Application. J Power Sources 2014;250:257-65.

[28] Zhang J, Zhou J, Wang D, Hou L, Gao F. Nitrogen and Sulfur Codoped Porous Carbon Microsphere: A High Performance Electrode in Supercapacitor. Electrochim Acta 2016;191:933-9.

[29] Renders T, Van den Bosch S, Koelewijn SF, Schutyser W, Sels BF. Lignin-first biomass fractionation: the advent of active stabilisation strategies. Energ Environ Sci 2017.

[30] Kai D, Tan MJ, Chee PL, Chua YK, Yap YL, Loh XJ. Towards Lignin-based Functional Materials in a Sustainable World. Green Chem 2016;18:1175-200.

[31] Suhas, Carrott PJ, Ribeiro Carrott MM. Lignin--from natural adsorbent to activated carbon: a review. Bioresour Technol 2007;98(12):2301-12.

[32] Chatterjee S, Saito T. Lignin-Derived Advanced Carbon Materials. ChemSusChem 2015;8:3941-58.

[33] Guo NN, Li M, Sun XK, Wang F, Yang R. Enzymatic Hydrolysis Lignin Derived Hierarchical Porous Carbon for Supercapacitors in Ionic Liquids with High Power and Energy Densities. Green Chem 2017;19:2595-602.

[34] Klose M, Reinhold R, Logsch F, Wolke F, Linnemann J, Stoeck U, et al. Softwood Lignin as a Sustainable Feedstock for Porous Carbons as Active Material for Supercapacitors Using an Ionic Liquid Electrolyte. ACS Sustainable Chem Eng 2017;5(5):4094-102.

[35] Jeon JW, Zhang L, Lutkenhaus JL, Laskar DD, Lemmon JP, Choi D, et al. Controlling porosity in lignin-derived nanoporous carbon for supercapacitor applications. ChemSusChem 2015;8(3):428-32.

[36] Zhang W, Zhao M, Liu R, Wang X, Lin H. Hierarchical porous carbon derived from lignin for high performance supercapacitor. Colloids and Surfaces A: Physicochemical and Engineering Aspects 2015;484:518-27.

[37] Zhang W, Lin H, Lin Z, Yin J, Lu H, Liu D, et al. 3 D Hierarchical Porous Carbon for Supercapacitors Prepared from Lignin through a Facile Template-Free Method. ChemSusChem 2015;8(12):2114-22.

[38] Pang J, Zhang W, Zhang H, Zhang J, Zhang H, Cao G, et al. Sustainable nitrogen-containing hierarchical porous carbon spheres derived from sodium lignosulfonate for high-performance supercapacitors. Carbon 2018;132:280-93.

[39] He Z-W, Yang J, Lü Q-F, Lin Q. Effect of Structure on the Electrochemical Performance of Nitrogen- and Oxygen-Containing Carbon Micro/Nanospheres Prepared from Lignin-Based Composites. ACS Sustainable Chem Eng 2013;1(3):334-40.

[40] Zhao H, Wang Q, Deng Y, Shi Q, Qian Y, Wang B, et al. Preparation of renewable lignin-derived nitrogen-doped carbon nanospheres as anodes for lithium-ion batteries. RSC Adv 2016;6(81):77143-50.

[41] Zhu L, Shen F, Smith RL, Yan L, Li L, Qi X. Black liquor-derived porous carbons from rice straw for high-performance supercapacitors. Chem Eng J 2017;316:770-7.

[42] Carrott PJM, Suhas, Carrott MMLR, Guerrero CI, Delgado LA. Reactivity and porosity development during pyrolysis and physical activation in CO_2 or steam of kraft and hydrolytic lignins. J Anal Appl Pyrolysis 2008;82(2):264-71.

[43] Li-Feng C, Lu Y, Yu L, Lou XW. Designed Formation of Hollow Particle-based Nitrogen-doped Carbon Nanofibers for High-performance Supercapacitors. Energ Environ Sci 2017;10: 1777-83.

[44] Zhu Y, Murali S, Stoller MD, Ganesh KJ, Cai W, Ferreira PJ, et al. Carbon-based Supercapacitors Produced by Activation of Graphene. Science 2011;332:1537-11541.

[45] Xie LJ, Sun GH, Su FY, Guo XQ, Kong QQ, Li XM, et al. Hierarchical Porous Carbon Microtubes Derived from Willow Catkins for Supercapacitor Applications. J Mater Chem A 2016;4:1637-46.

[46] Walters CC, Wang FC, Qian K, Wu C, Mennito AS, Wei Z. Petroleum alteration by thermochemical sulfate reduction – A comprehensive molecular study of aromatic hydrocarbons and polar compounds. Geochim Cosmochim Acta 2015;153:37-71.

[47] Dai J, Ni Y, Qin S, Huang S, Peng W, Han W. Geochemical characteristics of ultra-deep natural gas in the Sichuan Basin, SW China. PETROL EXPLOR DEVELOP 2018;45(4):619-28.

[48] Karan K, Mehrotra AK, Behie LA. On Reaction Kinetics for the Thermal Decomposition of Hydrogen Sulfide. AIChE J 1999;45(2):383-9.

[49] Chen JZ, Xu JL, Zhou S, Zhao N, Wong C-P. Nitrogen-doped Hierarchically Porous Carbon Foam: A Free-standing Electrode and Mechanical Support for High-performance Supercapacitors. Nano Energy 2016;25:193-202.

[50] Ren G, Li S, Fan Z-X, Warzywoda J, Fan Z. Soybean-derived Hierarchical Porous Carbon with Large Sulfur Loading and Sulfur Content for High-performance Lithium–sulfur Batteries. J Mater Chem A 2016;4: 16507-15.

[51] Zhao Y-Q, Lu M, Tao P-Y, Zhang Y-J, Gong X-T, Yang Z, et al. Hierarchically Porous and Heteroatom Doped Carbon Derived from Tobacco Rods for Supercapacitors. J Power Sources 2016;307:391-400.

[52] Xie B, Chen Y, Yu M, Sun T, Lu L, Xie T, et al. Hydrothermal Synthesis of Layered Molybdenum Sulfide/N-doped Graphene Hybrid with Enhanced Supercapacitor Performance. Carbon 2016;99:35-42.

[53] Li Z, Xu Z, Tan X, Wang H, Holt CMB, Stephenson T, et al. Mesoporous Nitrogen-rich Carbons Derived from Protein for Ultra-high Capacity Battery Anodes and Supercapacitors. Energ Environ Sci 2013;6:871-8.

[54] Qie L, Chen W, Xu H, Xiong X, Jiang Y, Zou F, et al. Synthesis of Functionalized 3D Hierarchical Porous Carbon for High-performance Supercapacitors. Energ Environ Sci 2013;6:2497-504.

[55] Ma X, Ning G, Wang Y, Song X, Xiao Z, Hou L, et al. S-doped Mesoporous Graphene Microspheres: A High Performance Reservoir Material for Li-S Batteries. Electrochim Acta 2018;269:83-92.

[56] Yang W, Yang W, Song A, Gao L, Su L, Shao G. Supercapacitance of Nitrogen-sulfur-oxygen Co-doped 3D Hierarchical Porous Carbon in Aqueous and Organic Electrolyte. J Power Sources 2017;359:556-67.

[57] Cheng P, Gao SY, Zang PY, Yang XF, Bai YL, Xu H, et al. Hierarchically Porous Carbon by Activation of Shiitake Mushroom for Capacitive Energy Storage. Carbon 2015;93:315-24.

[58] Feng HB, Hu H, Dong HW, Xiao Y, Cai YJ, Lei BF, et al. Hierarchical Structured Carbon Derived from Bagasse Wastes: A Simple and Efficient Synthesis Route and Its Improved Electrochemical Properties for High-performance Supercapacitors. J Power Sources 2016;302:164-73.

[59] Gao F, Qu JY, Geng C, Shao GH, Wu MB. Self-templating Synthesis of Nitrogen-decorated Hierarchical Porous Carbon from Shrimp Shell for Supercapacitors. J Mater Chem A 2016;4:7445-52.

[60] Gao F, Qu JY, Zhao ZB, Wang ZY, Qiu JS. Nitrogen-doped Activated Carbon Derived from Prawn Shells for High-performance Supercapacitors. Electrochim Acta 2016;190:1134-41.

[61] Huang Y, Peng L, Liu Y, Zhao G, Chen JY, Yu G. Biobased Nano Porous Active Carbon Fibers for High-Performance Supercapacitors. ACS Appl Mater Interfaces 2016;8:15205-15.

[62] Largeot C, Taberna PL, Gogotsi Y, Simon P. Microporous Carbon-Based Electrical Double Layer Capacitor Operating at High Temperature in Ionic Liquid Electrolyte. Electrochem Solid-State Lett 2011;14(12):A174-A6.

[63] Chmiola J, Largeot C, Taberna P-L, Simon P, Gogotsi Y. Desolvation of ions in subnanometer pores and its effect on capacitance and double-layer theory. Angew Chem Int Ed 2008;47(18):3392-5.

[64] Lin R, Huang P, Ségalini J, Largeot C, Taberna PL, Chmiola J, et al. Solvent effect on the ion adsorption from ionic liquid electrolyte into sub-nanometer carbon pores. Electrochim Acta 2009;54(27):7025-32.

[65] Dyatkin B, Gogotsi Y. Effects of structural disorder and surface chemistry on electric conductivity and capacitance of porous carbon electrodes. Faraday Discuss 2014;172:139-62.

[66] Lewandowski A, Olejniczak A, Galinski M, Stepniak I. Performance of Carbon–carbon Supercapacitors Based on Organic, Aqueous and Ionic Liquid Electrolytes. J Power Sources 2010;195:5814-9.

[67] Chen C, Yu D, Zhao G, Du B, Tang W, Sun L, et al. Three-dimensional Scaffolding Framework of Porous Carbon Nanosheets Derived from Plant Wastes for High-performance Supercapacitors. Nano Energy 2016;27:377-89.

[68] Wang HL, Li Z, Tak JK, Holt CMB, Tan X, Xu Z, et al. Supercapacitors Based on Carbons with Tuned Porosity Derived from Paper Pulp Mill Sludge Biowaste. Carbon 2013;57:317-28.

[69] Tian W, Gao Q, Tan Y, Yang K, Zhu L, Yang C, et al. Bio-inspired Beehive-like Hierarchical Nanoporous Carbon Derived from Bamboo-based Industrial By-product as a High Performance Supercapacitor Electrode Material. J Mater Chem A 2015;3:5656-64.

[70] Wang H, Xu Z, Kohandehghan A, Li Z, Cui K, Tan X, et al. Interconnected Carbon Nanosheets Derived from Hemp for Ultrafast Supercapacitors with High Energy. ACS Nano 2013;7(6):5131–41.

[71] Yang W, Yang W, Ding F, Sang L, Ma Z, Shao G. Template-free Synthesis of Ultrathin Porous Carbon Shell with Excellent Conductivity for High-rate Supercapacitors. Carbon 2017;111:419-27.